Research Article | Vol. 25, No. 20 | 2 Oct 2017 | OPTICS EXPRESS 23773
Optics EXPRESS

Dual polarization split lenses

AARÓN COFRÉ,[1,2,*] ASTICIO VARGAS,[2] FABIÁN A. TORRES-RUIZ,[2] JUAN CAMPOS,[3] ANGEL LIZANA,[3] MARÍA M. SÁNCHEZ-LÓPEZ,[4] AND IGNACIO MORENO[1]

[1]*Departamento de Ciencia de Materiales, Óptica y Tecnología Electrónica, Universidad Miguel Hernández de Elche, 03202 Elche, Spain*
[2]*Departamento de Ciencias Físicas, Universidad de La Frontera, Temuco, Chile*
[3]*Departamento de Física, Universidad Autónoma de Barcelona, Barcelona, Spain*
[4]*Instituto de Bioingeniería, Departamento de Física y Arquitectura de Computadores, Universidad Miguel Hernández de Elche, 03202 Elche, Spain*
[*]*acofre@umh.es*

Abstract: We report the realization of polarization sensitive split lens configurations. While split lenses can be used to easily generate different types of controlled structured light patterns, their realization has been limited so far to scalar beams. Here we propose and experimentally demonstrate their generalization to vectorial split lenses, leading to light patterns with customized intensity and state of polarization. We demonstrate how these polarization split lenses can be experimentally implemented by means of an optical system using two liquid crystal spatial light modulators, each one phase modulating one orthogonal polarization component. As a result, we demonstrate the experimental generation of vectorial beams with different shapes generated with these dual polarization split lenses. Excellent experimental results are provided in each case. The proposed technique is a simple method to generate structured light beams with polarization diversity, with potential applications in polarimetry, customized illuminators or quantum optics.

OCIS codes: (260.5430) Polarization; (050.1965) Diffractive lenses; (070.6120) Spatial light modulators.

References and links

1. J. Leach, B. Jack, J. Romero, A. K. Jha, A. M. Yao, S. Franke-Arnold, D. G. Ireland, R. W. Boyd, S. M. Barnett, and M. J. Padgett, "Quantum correlations in optical angle-orbital angular momentum variables," Science **329**(5992), 662–665 (2010).
2. M. McLaren, M. Agnew, J. Leach, F. S. Roux, M. J. Padgett, R. W. Boyd, and A. Forbes, "Entangled Bessel-Gaussian beams," Opt. Express **20**(21), 23589–23597 (2012).
3. R. Fickler, R. Lapkiewicz, S. Ramelow, and A. Zeilinger, "Quantum entanglement of complex photon polarization patterns in vector beams," Phys. Rev. A **89**(6), 060301 (2014).
4. T. Müller, C. Schumann, and A. Kraegeloh, "STED microscopy and its applications: new insights into cellular processes on the nanoscale," ChemPhysChem **13**(8), 1986–2000 (2012).
5. T. Vettenburg, H. I. C. Dalgarno, J. Nylk, C. Coll-Lladó, D. E. K. Ferrier, T. Čižmár, F. J. Gunn-Moore, and K. Dholakia, "Light-sheet microscopy using an Airy beam," Nat. Methods **11**(5), 541–544 (2014).
6. K. Henderson, C. Ryu, C. MacCormick, and M. G. Boshier, "Experimental demonstration of painting arbitrary and dynamic potentials for Bose–Einstein condensates," New J. Phys. **11**(4), 043030 (2009).
7. A. Turpin, J. Polo, Y. V. Loiko, J. Küber, F. Schmaltz, T. K. Kalkandjiev, V. Ahufinger, G. Birkl, and J. Mompart, "Blue-detuned optical ring trap for Bose-Einstein condensates based on conical refraction," Opt. Express **23**(2), 1638–1650 (2015).
8. P. J. Rodrigo, V. R. Daria, and J. Glückstad, "Four dimensional optical manipulation of colloidal particles," Appl. Phys. Lett. **86**(7), 074103 (2005).
9. D. B. Phillips, M. J. Padgett, S. Hanna, Y.-L. D. Ho, D. M. Carberry, M. J. Miles, and S. H. Simpson, "Shape-induced force fields in optical trapping," Nat. Photonics **8**(5), 400–405 (2014).
10. J. A. Rodrigo and T. Alieva, "Freestyle 3D laser traps: tools for studying light-driven particle dynamics and beyond," Optica **2**(9), 812–815 (2015).
11. V. G. Shvedov, A. V. Rode, Y. V. Izdebskaya, A. S. Desyatnikov, W. Krolikowski, and Y. S. Kivshar, "Selective trapping of multiple particles by volume speckle field," Opt. Express **18**(3), 3137–3142 (2010).
12. C. J. Cheng and J. L. Chern, "Symmetry property of a generalized Billet's N-split lens," Opt. Commun. **283**(19), 3564–3568 (2010).

#300587 https://doi.org/10.1364/OE.25.023773
Journal © 2017 Received 21 Jun 2017; revised 27 Jul 2017; accepted 27 Jul 2017; published 19 Sep 2017

Optics EXPRESS

13. C. J. Cheng and J. L. Chern, "Quasi Bessel beam by Billet's N-split lens," Opt. Commun. **283**(24), 4892–4898 (2010).
14. A. Lizana, A. Vargas, A. Turpin, C. Ramirez, I. Estevez, and J. Campos, "Shaping light with split lens configurations," J. Opt. **18**(10), 105605 (2016).
15. H. Rubinsztein-Dunlop, A. Forbes, M. V. Berry, M. R. Dennis, D. L. Andrews, M. Mansuripur, C. Denz, C. Alpmann, P. Banzer, T. Bauer, E. Karimi, L. Marrucci, M. Padgett, M. Ritsch-Marte, N. M. Litchinitser, N. P. Bigelow, C. Rosales-Guzmán, A. Belmonte, J. P. Torres, T. W. Neely, M. Baker, R. Gordon, A. B. Stilgoe, J. Romero, A. G. White, R. Fickler, A. E. Willner, G. Xie, B. McMorran, and A. M. Weiner, "Roadmap on structured light," J. Opt. **19**(1), 013001 (2017).
16. A. Cofré, A. Vargas, F. A. Torres-Ruiz, J. Campos, A. Lizana, M. M. Sánchez-López, and I. Moreno, "Quantitative performance of a polarization diffraction grating polarimeter encoded onto two liquid-crystal-on-silicon displays," Opt. Laser Technol. **96**, 219–226 (2017).
17. B. Khajavi and E. J. Galvez, "High-order disclinations in space-variant polarization," J. Opt. **18**(8), 084003 (2016).
18. I. Moreno, J. A. Davis, D. M. Cottrell, and R. Donoso, "Encoding high-order cylindrically polarized light beams," Appl. Opt. **53**(24), 5493–5501 (2014).
19. I. Moreno, J. A. Davis, T. M. Hernandez, D. M. Cottrell, and D. Sand, "Complete polarization control of light from a liquid crystal spatial light modulator," Opt. Express **20**(1), 364–376 (2012).
20. D. Maluenda, I. Juvells, R. Martínez-Herrero, and A. Carnicer, "Reconfigurable beams with arbitrary polarization and shape distributions at a given plane," Opt. Express **21**(5), 5432–5439 (2013).
21. X. Zheng, A. Lizana, A. Peinado, C. Ramírez, J. L. Martínez, A. Márquez, I. Moreno, and J. Campos, "Compact LCOS-SLM based polarization pattern beam generator," J. Lightwave Technol. **33**(10), 2047–2055 (2015).
22. M. M. Sánchez-López, A. Vargas, A. Cofré, I. Moreno, and J. Campos, "Simple spectral technique to identify the ordinary and extraordinary axes of a liquid crystal retarder," Opt. Commun. **349**, 105–111 (2015).
23. F. J. Martínez, A. Márquez, S. Gallego, J. Francés, I. Pascual, and A. Beléndez, "Effective angular and wavelength modeling of parallel aligned liquid crystal devices," Opt. Lasers Eng. **74**, 114–121 (2015).
24. J. P. Balthasar Mueller, N. A. Rubin, R. C. Devlin, B. Groever, and F. Capasso, "Metasurface polarization optics: Independent phase control of arbitrary orthogonal states of polarization," Phys. Rev. Lett. **118**(11), 113901 (2017).
25. F. Wyrowski, "Diffractive optical elements: iterative calculation of quantized, blazed phase structures," J. Opt. Soc. Am. **7**(6), 961–969 (1990).
26. J. A. Davis, W. V. Brandt, D. M. Cottrell, and R. M. Bunch, "Spatial image differentiation using programmable binary optical elements," Appl. Opt. **30**(32), 4610–4614 (1991).
27. D. M. Cottrell, J. A. Davis, T. R. Hedman, and R. A. Lilly, "Multiple imaging phase-encoded optical elements written as programmable spatial light modulators," Appl. Opt. **29**(17), 2505–2509 (1990).
28. M. W. Beijersbergen, R. P. C. Coerwinkel, M. Kristensen, and J. P. Woerdman, "Helical-wavefront laser beams produced with a spiral phaseplate," Opt. Commun. **112**(5–6), 321–327 (1994).
29. A. Peinado, A. Lizana, A. Turpin, C. Iemmi, T. K. Kalkandjiev, J. Mompart, and J. Campos, "Optimization, tolerance analysis and implementation of a Stokes polarimeter based on the conical refraction phenomenon," Opt. Express **23**(5), 5636–5652 (2015).
30. Q. Zhan, "Cylindrical vector beams: From mathematical concepts to applications," Adv. Opt. Photonics **1**(1), 1–57 (2009).
31. W. Shu, X. Ling, X. Fu, Y. Liu, Y. Ke, and H. Luo, "Polarization evolution of vector beams generated by q-plates," Photon. Res. **5**(2), 64–72 (2017).
32. X. Yi, Y. Liu, X. Ling, X. Zhou, Y. Ke, H. Luo, S. Wen, and D. Fan, "Hybrid-order Poincaré sphere," Phys. Rev. A **91**(2), 023801 (2015).
33. I. Moreno, M. M. Sánchez-López, K. Badham, J. A. Davis, and D. M. Cottrell, "Generation of integer and fractional vector beams with q-plates encoded onto a spatial light modulator," Opt. Lett. **41**(6), 1305–1308 (2016).
34. P. Li, Y. Zhang, S. Liu, C. Ma, L. Han, H. Cheng, and J. Zhao, "Generation of perfect vectorial vortex beams," Opt. Lett. **41**(10), 2205–2208 (2016).

1. Introduction

The generation of structured light has become a very relevant topic in a number of different areas including quantum optical experiments [1–3], microscopy systems with enhanced resolution [4,5] or in optical trapping [6–11]. Structured light is typically achieved by properly designing computer generated holograms (CGH), which are then displayed onto spatial light modulators (SLM). However, the design of such CGH usually involves iterative processes, required to take into account the usual modulation limitations of SLM (phase-only displays are commonly employed as SLMs). Recently, a powerful strategy to design CGH for structured light generation without iterative methods was proposed, based on the concept of split lens configurations [12,13]. The experimental realization of split-lens using a phase-only

Optics EXPRESS

SLM has been demonstrated recently, and various different optical elements have been shown to highlight the interest of the method [14].

Moreover, in the last years there is a great interest in producing vector beams and achieving polarization control [15]. In this work, we apply an optical arrangement that uses two SLMs to independently control two linear polarizations with two independent phase-only CGHs. Then, we apply this system to generate different kinds of polarization selective split lenses, as well as to demonstrate the generation of vector beams encoded onto such lenses. Therefore, this combined method leads to a simple method to generate customized light distributions with polarization control.

The paper is organized as follows: after this introduction, Section 2 describes the optical system, and presents a first set of experimental results that demonstrate the realization of polarization CGHs. Then, in Section 3 we review the split lens concept, and in Section 4 we generalize them to vectorial lenses and present different cases with different polarization diversity. Section 5 present the combination of split lenses with spiral phases in order to generate vector beams. Finally, Section 6 present the conclusions of the work.

2. Optical system

Figure 1 shows the optical setup, which was previously introduced in [16]. It uses two phase-only parallel-aligned LCoS-SLMs, arranged in a Z architecture, in order to independently modulate two orthogonal polarization components, as introduced in [17]. Such modulation capability can be achieved with other SLM based optical arrangements [18–21]. However, this Z optical architecture is very robust, stable, and efficient since it has a common path for both polarization components, and no beam splitters are required.

The system is illuminated with a He-Ne laser λ = 633 nm, which is spatially filtered and collimated through lens L_1. A first polarizer (P_1) controls orientation of the electric field of the light incident on the system. In each LCoS device, the incident ray and the reflected ray form an angle of around 11°. Although non-normal incidence affects the modulation provided by the display, such small angle of incidence produces only a very small variation [22,23]. Both LCoS displays are located in conjugated planes through a 4f system, composed of two lenses L_2 and L_3, both with a focal length of f = 200 mm. Thus, the pattern addressed to LCoS1 display is imaged onto LCoS2 display with minus one magnification. This inversion must be compensated in the phase-only masks design, in order to obtain the expected results.

The SLMs are parallel-aligned LCoS displays from Holoeye, model Pluto, with 1920 × 1080 pixels, with an 8 μm pixel pitch. In both displays, the liquid crystal director is aligned horizontally with respect to laboratory framework. The retardance was calibrated at room temperature as a function of the addressed gray level in both modulators for the operating wavelength of 633 nm [16]. The phase modulation produced in both displays is only for the linear polarization component parallel to LC director, and therefore only modulates the horizontal component of polarization. Thus, LCoS1 modulates the horizontal polarization component of the incident initial beam, leaving the vertical component unaffected. Then, the reflected beam goes through a half-wave-plate retarder (HWP) placed after L_3, and oriented at 45° relative to the horizontal. This HWP transforms the input horizontal polarization component into vertical polarization component and vice versa. Thus, the LCoS2 display phase modulates the initially vertical polarization component of the incident beam, leaving unaffected the initially horizontal polarization component (which was previously modulated by LCoS1). This way, we can modulate independently both polarization components with two different phase masks addressed to LCoS1 and LCoS2 respectively. The use of the HWP in the system avoids the rotation of LCoS2 display, as it was done in [17] by Khajavi and Galvez. The input polarizer (P_1) is selected oriented at 45°, so the vertical and horizontal components of the light beam have the same magnitude.

Finally, a lens L_4 located on the beam reflected from LCoS2 is placed to focus the back focal plane onto a CCD camera, Basler piA1000 60gm. A second polarizer (P_2) is used as an

Optics EXPRESS

analyzer, placed in front to the camera. When P_2 is oriented at 0°, the pattern encoded on LCoS1 is the one that is transmitted, while the pattern encoded on LCoS2 is transmitted when P_2 is oriented at 90°. When P_2 is oriented at ± 45° both patterns are visible and, if they overlap, they are added coherently.

In some experiments (only those shown in Section 5), we also include a quarter-wave plate (QWP) in the beam reflected form LCoS2 display. This is useful when we want to generate vector beams combined with the encoded split lenses. In this situation, spiral phase patterns must be encoded onto circularly polarized beams. We use this QWP, oriented at 45°, to transform the linear vertical and horizontal polarization states into the two circular states, following a scheme similar to that in [18].

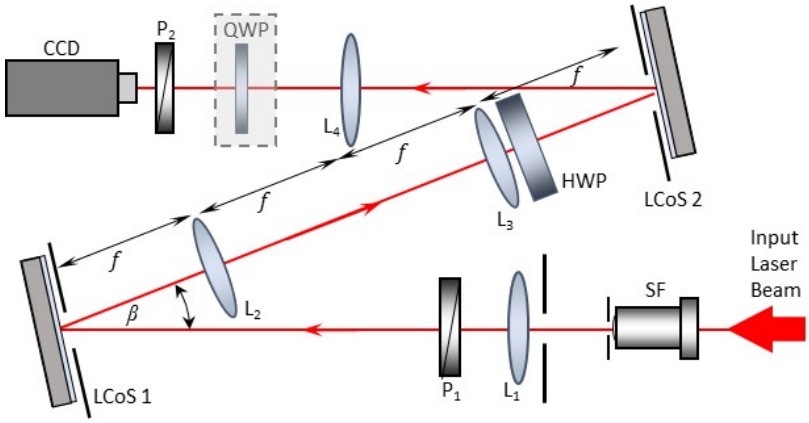

Fig. 1. Optical system. SF is a spatial filter. P_1 and P_2 are linear polarizers. LCoS1 and LCoS2 are liquid-crystal on silicon displays, both with the LC director oriented horizontally. L_1 collimates the input beam. L_2 and L_3 compose a 4f system where both displays are in conjugated planes. L_4 is used to focus the final plane on the CCD camera. In some experiments, a quarter-wave plate (QWP) is also included in the system.

In order to prove the polarization control achieved with this system, we first demonstrated a polarization CGH, where the response is different depending on the input state of polarization. Polarization sensitive holograms that show a different response for different input polarizations have been demonstrated with meta-surfaces [24], as well as with a different SLM based optical arrangement [19]. Here we use the above-described optical arrangement in Fig. 1. For that purpose, two phase-only Fourier transform CGHs were designed and implemented by LCoS1 and LCoS2 displays respectively. The CGH encoded in the LCoS1 display encodes the texts UFRO and UAB. This CGH therefore affects only the incident horizontal linear polarization, which emerges the system vertically polarized. On the contrary, the CGH displayed on LCoS2 display encodes the texts UFRO and UMH on the initially vertical linear polarization, which emerges the system horizontally polarized.

The experimental results in Fig. 2 confirm the capability to produce polarized CGHs with the system in Fig. 1. The input polarizer P_1 is oriented at 45°, so the horizontal and vertical components have the same weight. Therefore, the pattern UFRO gets contributions from both holograms, thus getting twice the intensity of the UAB and UMH patterns. In Figs. 2(a) and 2(c) the analyzer P_2 is oriented vertical and horizontal respectively. In these cases, the patterns UMH and UAB are extinguished in one case respectively. On the contrary, in Figs. 2(b) and 2(d) P_2 is oriented at ± 45°. Then all three patterns are present in both images. The patterns UMH and UAB appears with half intensity, since they are horizontally and vertically polarized. The pattern UFRO projects in all cases with the same intensity since it is circularly polarized. The speckle that appears on these reconstructions is due to random noise that was added to the letters when designing the CGH, in order to avoid the edge enhancement characteristic of a phase-only hologram [25].

Optics EXPRESS

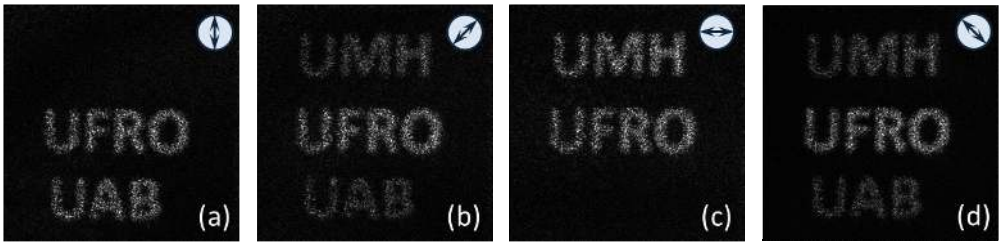

Fig. 2. Demonstration of the polarization CGH. LCoS1 and LCoS2 SLMs display two different holograms, encoding the words UFRO - UAB and UMH - UFRO respectively. The CGH reconstruction is shown for different orientations of the analyzer (P_2), indicated on top.

3. Split lens design

As mentioned in the introduction, the split lens concept has been recently introduced [12–14]. With this approach, a composite diffractive lens is generated as the combination of multiple individual lenses, each one having a different location of its center. Note that a similar approach was introduced much earlier, to produce image differentiation [26]. In a split lens composed of a discrete number of lenses, the center of each individual lens is defined by a vector with coordinates $\mathbf{d}_m = (d_{mx},d_{my})$, where the index m denotes each of the individual lenses. But the split lens can be made more general by generating a continuous variation of the lens center location, in order to create an arbitrary light distribution. The split lens complex amplitude can be written in a general form $U(r,\theta)$ as [14]:

$$U(r,\theta) = \exp\left[i\frac{\pi}{\lambda f}\left|\mathbf{r} - \mathbf{d}_m(\theta)\right| \right], \tag{1}$$

where $\mathbf{r} = (x,y)$ is the vector denoting the spatial coordinates in the lens plane (in our case the SLM plane). θ denotes the azimuthal coordinate, $\tan\theta = y/x$, and f denotes the lens focal length. In this work, we restrict the results for a single focal plane, and therefore we employ this single constant focal length, but in general, a variable focal length can be also applied, as demonstrated in [14]. Finally, the function $\mathbf{d}_m$ is a continuous function that defines the location of the center of the split lenses encoded onto each azimuthal direction θ.

Figure 3 shows three different examples. In Figs. 3(a) and 3(b), the split lens is discrete, with 5 sectors (thus Eq. (1) becomes a piecewise-defined function). Therefore, the function $\mathbf{d}_m(\theta)$, $m = 0,1,2,3,4$ for these two phase masks is given by

$$\mathbf{d}_m(\theta) = \left(d\cos(\theta_m), d\sin(\theta_m)\right), \tag{2}$$

where $d = 0.235$ mm for Fig. 3(a) and $d = 0.600$ mm for Fig. 3(b). The five sectors cover angular ranges of 72°, with the lens centers located at angles $\theta_1 = 36°$, $\theta_2 = 108°$, $\theta_3 = 180°$, $\theta_4 = 252°$ and $\theta_5 = 324°$ respectively. Therefore, these split lenses will produce five different focal spots at the same focal plane, displaced from the center in angles defined by Eq. (2).

Finally, Fig. 3(c) shows a continuous version, where now the location of the center of the lens is maintained at a fixed radius, $d = 0.6$ mm, but the angular position varies continuously as the azimuthal coordinate, i.e., now the function $\mathbf{d}_m = (\theta)$ is given by $\mathbf{d}_m = (d\cos\theta, d\sin\theta)$. This lens produces a focalization in the form of a ring of light, as presented by Lizana *et al* in [14]. However, all the results presented there were scalar lenses. What we present next is the combination of such novel types of lenses in the polarization system in Fig. 1, to generate customized polarized structured light.

Optics EXPRESS

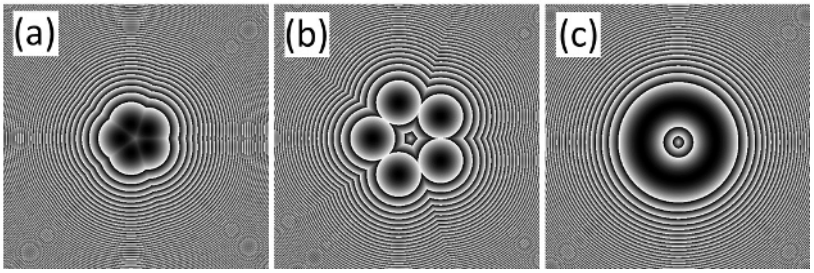

Fig. 3. Three different example designs of split lenses. (a) Segmented lens with 5 sectors with the centers located with equi-angular separation and small radius separation. (b) Segmented lens with the same 5 sectors and angular directions, but with larger radial separation. (c) Split lens with continuous angular rotation of the center.

4. Polarization split lenses

In this section, we present the experimental realization of different types of structured light patterns with polarization diversity, based on the implementation of split lenses in the system in Fig. 1. We design a different lens configuration for each display, so a different lens affects the vertical and the horizontal linear polarizations. As a result, we obtain interesting cases with different polarization and intensity distributions in the focal plane. Let us note that, since now we encode lenses directly on the LCoS displays, we do not need to use the physical lens L_4 in Fig. 1. A focal length $f = 100$ mm is encoded for all the results presented next. Although this long focal length makes the system long and more sensitive to vibrations, we selected this value to avoid secondary focalizations arising from aliasing effects [27]. In addition, alignment of the split lenses in each SLM is easier since the phase profiles vary slowly.

4.1 Multi-focalization with polarization diversity

The first case we show consists in a multiple focalization a discrete split lens composed of 5 angular sectors, creating a multiple focalization on the vertices of a pentagon, but with polarization control over the size of the shape. For this purpose, we generated two segmented split lenses as those in Fig. 3(a) and 3(b). Figure 4 presents the central part of the gray-level masks addressed to LCoS1 and LCoS2 displays and their corresponding experimental images captured at the CCD detector for four different orientations of the final polarizer (P_2).

Moreover, three cases are studied. Whereas the split lens addressed to LCoS1 display (modulating the vertical polarization) remains constant during all the experiments, with a constant value $d = 0.6$ mm, we set three different split lenses on the LCoS2 display (modulating the horizontal polarization), with values $d = 0.2$ mm, $d = 0.5$ mm and $d = 1.0$ mm respectively. The images in the three rows in Fig. 4 correspond to these three cases.

For instance, when the analyzer is oriented vertically [Figs. 4(c), 4(i) and 4(o)], the pattern always shows the same size. However, when the analyzer is oriented horizontally [Figs. 4(e), 4(k) and 4(q)], we reproduce the same pattern, but with different size. When the analyzer is oriented at ± 45°, then the two patterns are visible with equal intensity. Note that the relative intensity of the vertical and horizontal polarizations structures can be adjusted simply by properly orienting the polarizers P_1 or P_2.

Figure 5 shows some equivalent results, but now we encode the same radius d for the two split lenses, but change the angular orientation of the lenses encoded in the horizontal polarization. The angular separation between the lenses encoded in LCoS1 and LCoS2 displays is of $\alpha = 12°$, $\alpha = 30°$ and $\alpha = 60°$ in the results in the first, second and third rows in Fig. 5. Again, when the analyzer is oriented either vertical [Fig. 5(c), 5(i) and 5(o)] or horizontal [Fig. 5(e), 5(k) and 5(q)], only one set of focalizations is observed, corresponding to a split lens with five sectors. On the contrary, when the analyzer is oriented at ± 45°, the two patterns are visible with equal intensity, and we get 10 focal spots.

Optics EXPRESS

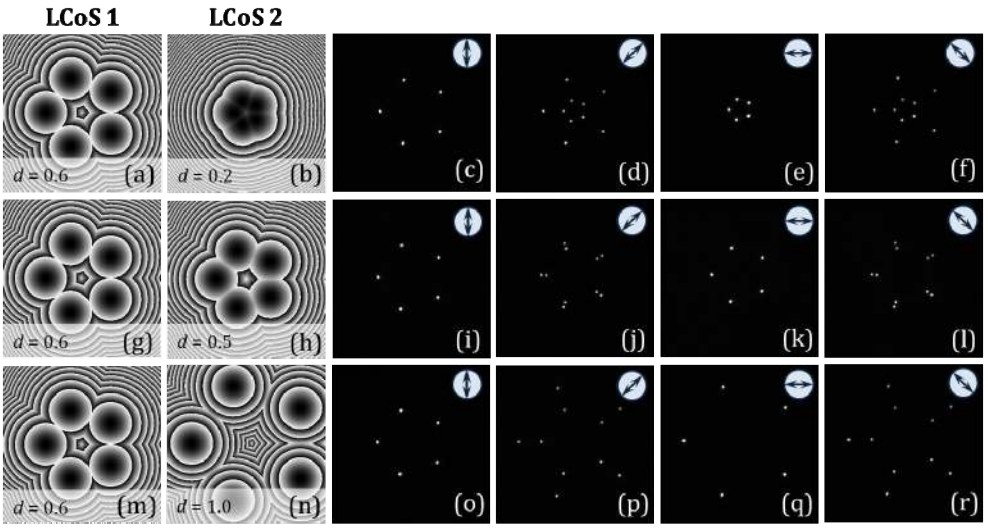

Fig. 4. Results with segmented polarization Billet split lenses with five focal spots distributed angularly. Here the vertical polarization component encodes a separation d = 0.6 mm, while the horizontal polarization component encodes a separation of d = 0.2 mm (first row), d = 0.5 mm (second row) and d = 1.0 mm (third row) (see Visualization 1). The symbol over the experimental captures indicates the orientation of the analyzer.

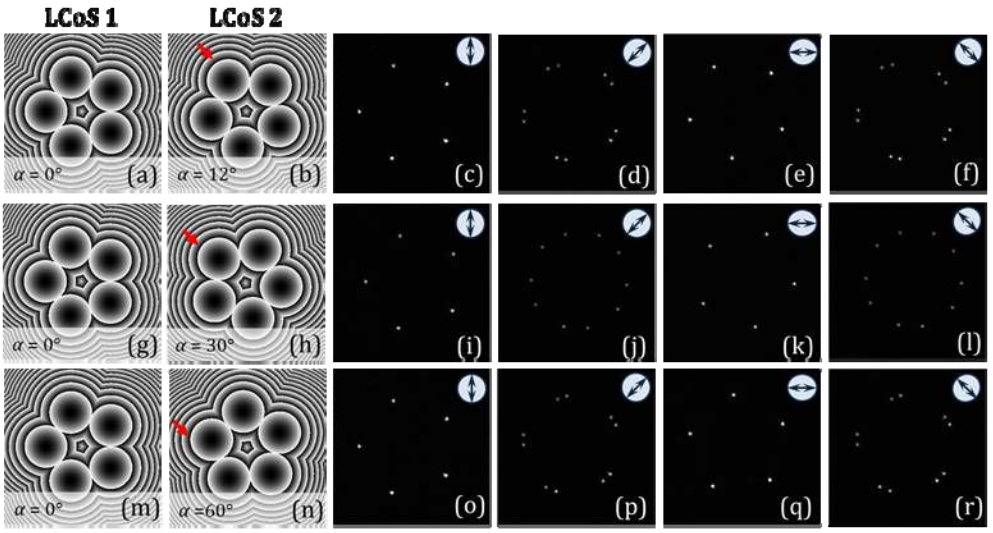

Fig. 5. Results with segmented polarization split lenses with five focal spots distributed angularly. Here both polarization components encode the same separation d = 0.6 mm, but there is an angular separation α = 12° (first row), α = 30° (second row) and α = 60° (third row). The red arrows marked in (b), (h) and (n) indicate the center of one specific lens, to easily visualize this rotation (see Visualization 2). The symbol over the experimental captures indicates the orientation of the analyzer.

4.2 Annular focalization with two polarizations

The next case we show consists in creating a focalization in the form of a ring of light. This type of shape has been extensively studied for applications in STED microscopy or in optical trapping, and they have been generated in a variety of techniques including vortex creating spiral phase masks [28], or conical refraction [29]. Here we create such type of focalization

Optics EXPRESS

employing a continuous split lens, as those demonstrated previously in [14] for the scalar case. The novelty here is that we generate such pattern but adding control of the state of polarization. Figure 6 shows the two phase-masks addressed to LCoS1 and LCoS2 displays, and the corresponding experimental results.

The first row in Fig. 6 corresponds to a case where a single circle of light is generated. This is achieved by designing phase masks like those in Fig. 6(a) and 6(b), where continuous split lenses are encoded, but only on half plane. The other half-plane encodes a random pattern. This way each display generates only half circle of light. The diameter of the split lens displacement is selected equal for both masks, d = 0.6 mm. The combined result is a focalization in the form of the complete circle of light, but half circle of light is polarized in the vertical direction, while the other half is polarized in the horizontal direction. This is verified when the analyzer P_2 is rotated. When it is oriented horizontal, only the upper half of the circle appears [Fig. 6(c)], and when it is oriented vertical, the other half circle appears [Fig. 6(e)]. As expected, when the analyzer is oriented at ± 45°, the circle appears complete, as shown in Figs. 6(d) and 6(f)

The second row shows a different case where we implemented two continuous split lenses, now covering the complete lens plane, but with different displacement parameter d for each polarization. The lens in LCoS1 display is selected with d = 0.6 mm [Fig. 6(g)], while the lens in LCoS2 display is selected with d = 0.8 mm [Fig. 6(h)]. The focalization now shows two rings with different diameter. When the analyzer is either vertical or horizontal, only one ring appears. When the analyzer is oriented at ± 45°, then the two rings of light are visible.

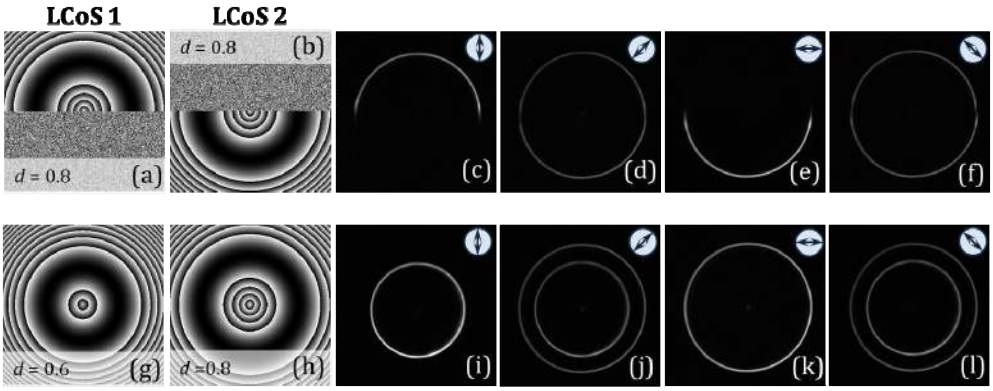

Fig. 6. Results with continuous polarization split lenses. The first row shows results for half-plane lenses with the same displacement d = 0.6 mm (see Visualization 3). The second row shows results for two complete lenses with different displacements d = 0.6 mm for the vertical polarization and d = 0.8 mm for the horizontal polarization. The symbol over the experimental captures indicates the orientation of the analyzer.

5. Split lenses for the generation of vector beams

This last section of the paper is devoted to the design of split lenses that additionally encode vector beams. Recently, there has been a great amount of works dealing with the generation of such vector beams with different techniques [30,31]. Here we present additional relevant results where we show the potential of the split lenses when combined with vector beams.

In particular, we exploit the fact that pure vector beams are obtained as the linear combination of two circularly polarized light beams carrying opposite azimuthal phase patterns $\exp(\pm i\ell\theta)$, where ℓ is known as the topological charge. If azimuthal (spiral) phases with different charge are encoded onto the two circular states, then hybrid vector beams are obtained [32]. As mentioned in Section 2, we modify the optical system by adding a QWP on

Optics EXPRESS

the beam reflected from LCoS2 display. This QWP is oriented with the principal axis oriented at 45° to the horizontal direction. This way, the phase patterns addressed to the LCoS1 and LCoS2 displays, initially encoded on the linear vertical and horizontal polarization components, are now encoded onto the final right handed and left handed circular polarization components. This way, we are able to combine the dual polarization Billet split lenses with spiral phases generating vector beams. The result can be written in a vectorial form as the following Jones vector:

$$\mathbf{V} = U_R(r,\theta)\exp(i\ell_R\theta)|R\rangle + U_L(r,\theta)\exp(i\ell_L\theta)|L\rangle, \tag{3}$$

where $|R\rangle$ and $|L\rangle$ are the Jones vectors corresponding to right and left circularly polarized light, $U_R(r,\theta)$ and $U_L(r,\theta)$ are the split lenses encoded onto LCoS1 and LCoS2 displays, that now are encoded in the right and left circular states, ℓ_R and ℓ_L are the topological charges encoded onto the right and left circular states. If the values of ℓ_R and ℓ_L are equal but with opposite sign, the system is then encoding an equivalent *q*-plate element [33] combined with the encoded split lens.

Figure 7 shows an example of this powerful combination. Here we generate the same continuous split lens for both displays, with constant displacement d = 0.6 mm, in order to generate a circle of light. However, we now combine it with spiral phases of different topological charges. The phase masks shown on top of Fig. 7 correspond to charges $\ell = \pm 2$, ± 4. These masks show the pattern of the continuous split lens, but it is modified with a spiral pattern. The experimental results shown in different rows of Fig. 7 correspond to different combinations of these masks when displayed onto the two LCoS displays.

As noted in [32], the different spiral phases encoded onto the circular polarization components induces an azimuthal rotation on the linear polarization, and the rotation along the complete circle is proportional to the difference $\ell_R - \ell_L$. This is shown for instance in the results in the first row in Fig. 7, where $\ell_R = 2$ and $\ell_L = 4$. A continuous polarization rotation of 180° is expected along the circle of light. This expected pattern in shown in Fig. 7(c), where the red arrows indicate the expected local state of polarization. The experimental result in Figs. 7(d) and 7(e) verify this result. Here for simplicity we present only the results with the analyzer oriented at ± 45°. Note the equivalence of the polarization pattern in Fig. 7(c) with that generated by conical refraction [28].

The additional cases shown in Fig. 7 are variations of this case using different values of the topological charges. In the cases shown in the second and fourth rows, the encoded charges are $\ell = \pm 2$ and $\ell = \pm 4$ respectively, thus generating a pure vector beam. For instance, the expected pattern drawn in Fig. 7(h) follows an azimuthal polarization along the circle of light generated by the split lens, since the polarization rotation completes 360° along the azimuthal coordinate. Note that a constant phase can be added to one of the phase masks addressed to each LCoS display in order to change the origin of rotation, and therefore change the polarization pattern. For instance the azimuthal polarization in Fig. 7(h) can be changed to a radial polarization simply by adding a constant phase of 180° to the mask displayed in Fig. 7(g). The number of cycles of polarization rotation along the circle of light varies proportional to $\ell_R - \ell_L$. In the four rows in Fig. 7, the values of the difference in topological charges change as $\ell_R - \ell_L$ = 2,3,4 and 8 respectively. Note how the corresponding number of dark lobes along the circle of light in the experimental results in the last two columns is half the value of $\ell_R - \ell_L$.

This above-discussed method leads to a larger versatility and control in comparison to other techniques such as *q*-plates [33], conical refraction [29], or perfect vectorial vortex beams [34]. Since the function $\mathbf{d}_m(\theta)$ in Eq. (1) can be customized to generate different

shapes, this approach allows the generation of vector beams with focalization shapes that can be different to the typical circular shapes achieved with these above-mentioned techniques.

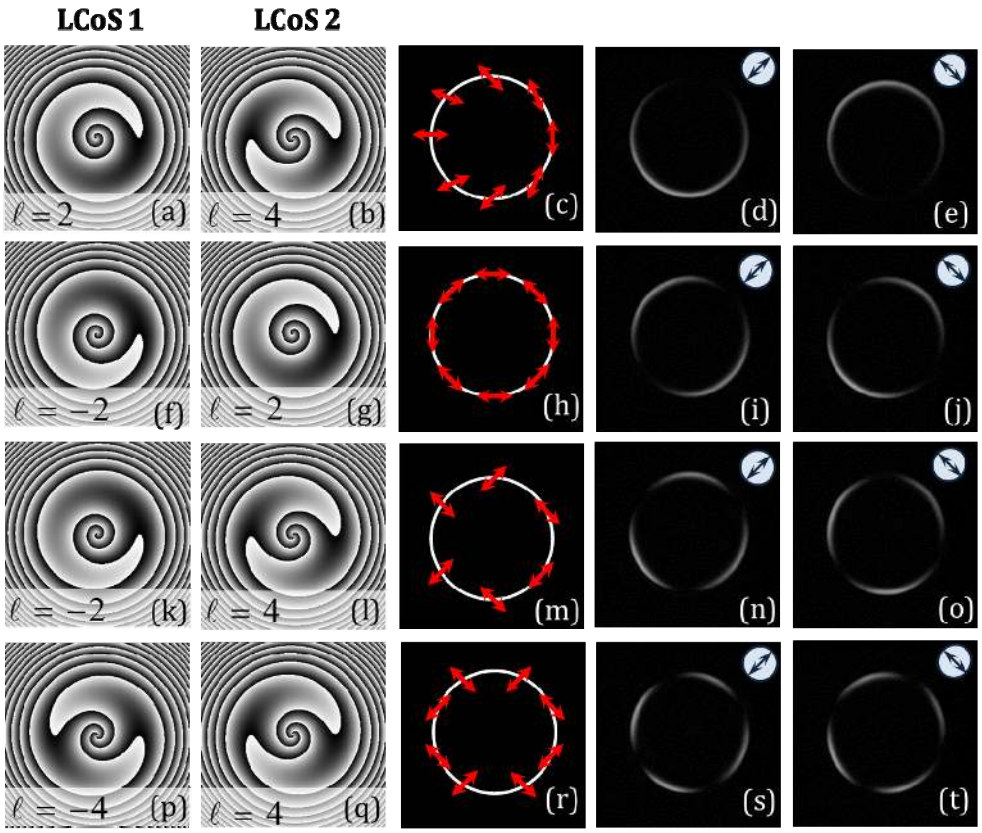

Fig. 7. Results with a continuous polarization split lens with d = 0.6 mm, combined with spiral phases of different topological charges to generate vector beams. The two left columns shows the two phase-masks displayed in each case, the central column shows the expected polarization pattern, and the two right columns show the corresponding experimental result obtained with the analyzer oriented at ± 45°.

6. Conclusions

In summary, we have combined the technique of split lenses with a dual polarization system capable to independently modulate two orthogonal polarizations. This way we are able to extend the split lens concept to a more general vectorial light beam description, and design customized structured polarized light patterns.

We first demonstrated the realization of polarization diffractive elements with the proper combination of two phase-only CGHs. Then, we showed how the same system is useful for generating different simple structured light patterns with polarization diversity. We demonstrated some simple cases of discrete and continuous split lenses, with polarization control. Next, we have combined the split lenses with spiral phase patterns, to show the experimental realization of light intensity patterns with structured vector polarization. Note that this proof of concept provided in this work is a very versatile tool for light control. Split lenses allow creating arbitrary intensity patterns. Moreover, the dual polarization modulation provided by the two SLMs allows a full control of the state of polarization on these patterns.

Thus, this approach can be very useful for the generation of arbitrary light patterns, and can be easily extended to other shapes different to those here presented, including 3D

Optics EXPRESS

intensity and polarization profiles around the focal plane, that could be employed for applications such as in optical microscopy, optical trapping, and optical polarimetry, among others.

Funding:

Ministerio de Economía, Industria y Competitividad of Spain and European Union (MIMECO/FEDER, grants FIS2015-66328-C3-3-R and FIS2015-66328-C3-1-R); Fondo Nacional de Desarrollo Científico y Tecnológico, Chile (FONDECYT, grant 1151290); Generalitat Valenciana, Santiago Grisolia Program (grant 2015/073).